Brain Advance Access published September 20, 2013

BRAIN
A JOURNAL OF NEUROLOGY

Periventricular heterotopia in 6q terminal deletion syndrome: role of the *C6orf70* gene

Valerio Conti,[1,2,*] Aurelie Carabalona,[3,4,*] Emilie Pallesi-Pocachard,[3,4] Elena Parrini,[1] Richard J. Leventer,[5,6,7] Emmanuelle Buhler,[8] George McGillivray,[9] François J. Michel,[3,4] Pasquale Striano,[10] Davide Mei,[1] Françoise Watrin,[3,4] Stefano Lise,[11] Alistair T. Pagnamenta,[11] Jenny C. Taylor,[11] Usha Kini,[12] Jill Clayton-Smith,[13] Francesca Novara,[14] Orsetta Zuffardi,[14,15] William B. Dobyns,[16] Ingrid E. Scheffer,[17,18] Stephen P. Robertson,[19] Samuel F. Berkovic,[17] Alfonso Represa,[3,4] David A. Keays,[20] Carlos Cardoso[3,4,†] and Renzo Guerrini[1,2,†]

1 Paediatric Neurology and Neurogenetics Unit and Laboratories, A. Meyer Children's Hospital – Department of Neuroscience, Pharmacology and Child Health, University of Florence, 50139, Florence, Italy
2 IRCCS Stella Maris Foundation, 56128, Pisa, Italy
3 INSERM, INMED UMR901, Parc Scientifique de Luminy, BP 13, 13273 Marseille, France
4 Université Aix-Marseille, 13273, Marseille, France
5 Department of Neurology, Royal Children's Hospital, Parkville Victoria 3052, Australia
6 Murdoch Children's Research Institute, Parkville Victoria 3052 Australia
7 Department of Paediatrics, University of Melbourne, Victoria 3010 Australia
8 Plateforme postgenomique INMED-INSERM, Parc Scientifique de Luminy, BP 13, 13273, Marseille, France
9 Victorian Clinical Genetics Services, Murdoch Children's Research Institute, Victoria 3052 Australia
10 Paediatric Neurology and Muscular Diseases Unit, Department of Neurosciences, Rehabilitation, Ophtalmology, Genetics, Maternal and Child Health, University of Genoa, "G. Gaslini" Institute, 16147 Genova, Italy
11 NIHR Biomedical Research Centre, Wellcome Trust Centre for Human Genetics, Oxford, OX3 7BN, UK
12 Department of Clinical Genetics, Oxford Radcliffe NHS Trust, Oxford OX3 9DU, UK
13 Genetic Medicine, St Mary's Hospital, University of Manchester, M13 9WL, UK
14 Department Molecular Medicine, University of Pavia, 27100, Pavia, Italy
15 IRCCS Casimiro Mondino Foundation, 27100, Pavia, Italy
16 Centre for Integrative Brain Research Seattle Children's Research Institute Seattle WA 98101, USA
17 Epilepsy Research Centre, Department of Medicine, University of Melbourne, Austin Health, Victoria 3010, Australia
18 Florey Institute for Neuroscience and Mental Health, and Department of Paediatrics, University of Melbourne, Royal Children's Hospital, Parkville Victoria 3052 Australia
19 Department of Paediatrics and Child Health, Dunedin School of Medicine University of Otago, Dunedin, 9054, New Zealand
20 Research Institute of Molecular Pathology, 1030, Vienna, Austria

*These authors contributed equally to this work.
†These authors contributed equally to this work.

Correspondence to: Prof. Renzo Guerrini,
Paediatric Neurology and Neurogenetics Unit and Laboratories,
A. Meyer Children's Hospital Department of Neuroscience,
Pharmacology and Child Health,
University of Florence,
Viale Pieraccini 24, 50139,
Florence, Italy
E-mail: r.guerrini@meyer.it

Correspondence may also be addressed to: Dr. Carlos Cardoso, INMED INSERM U901, Parc Scientifique de Luminy, BP 13, 13273 Marseille, France,
E-mail: carlos.cardoso@inserm.fr

Received March 28, 2013. Revised July 16, 2013. Accepted July 19, 2013.
© The Author (2013). Published by Oxford University Press on behalf of the Guarantors of Brain. All rights reserved.
For Permissions, please email: journals.permissions@oup.com

Downloaded from http://brain.oxfordjournals.org/ by guest on September 22, 2013

Periventricular nodular heterotopia is caused by defective neuronal migration that results in heterotopic neuronal nodules lining the lateral ventricles. Mutations in filamin A (*FLNA*) or ADP-ribosylation factor guanine nucleotide-exchange factor 2 (*ARFGEF2*) cause periventricular nodular heterotopia, but most patients with this malformation do not have a known aetiology. Using comparative genomic hybridization, we identified 12 patients with developmental brain abnormalities, variably combining periventricular nodular heterotopia, corpus callosum dysgenesis, colpocephaly, cerebellar hypoplasia and polymicrogyria, harbouring a common 1.2 Mb minimal critical deletion in 6q27. These anatomic features were mainly associated with epilepsy, ataxia and cognitive impairment. Using whole exome sequencing in 14 patients with isolated periventricular nodular heterotopia but no copy number variants, we identified one patient with periventricular nodular heterotopia, developmental delay and epilepsy and a *de novo* missense mutation in the chromosome 6 open reading frame 70 (*C6orf70*) gene, mapping in the minimal critical deleted region. Using immunohistochemistry and western blots, we demonstrated that in human cell lines, C6orf70 shows primarily a cytoplasmic vesicular *puncta*-like distribution and that the mutation affects its stability and subcellular distribution. We also performed *in utero* silencing of *C6orf70* and of *Phf10* and *Dll1*, the two additional genes mapping in the 6q27 minimal critical deleted region that are expressed in human and rodent brain. Silencing of *C6orf70* in the developing rat neocortex produced periventricular nodular heterotopia that was rescued by concomitant expression of wild-type human C6orf70 protein. Silencing of the contiguous *Phf10* or *Dll1* genes only produced slightly delayed migration but not periventricular nodular heterotopia. The complex brain phenotype observed in the 6q terminal deletion syndrome likely results from the combined haploinsufficiency of contiguous genes mapping to a small 1.2 Mb region. Our data suggest that, of the genes within this minimal critical region, *C6orf70* plays a major role in the control of neuronal migration and its haploinsufficiency or mutation causes periventricular nodular heterotopia.

Keywords: 6q terminal deletion syndrome; *C6orf70* gene; brain malformations; periventricular nodular heterotopia; epilepsy

Abbreviations: CGH = comparative genomic hybridization; PNH = periventricular nodular heterotopia; RFP = red fluorescent protein

Introduction

The development of the human cerebral cortex is a complex dynamic process that can be broken down into partially overlapping stages, occurring during several gestational weeks. Genetic or acquired factors that impair this process often result in epileptogenic brain malformations, that represent a major cause of intellectual disabilities, severe epilepsy and reproductive disadvantage (Guerrini *et al*., 2008; Barkovich *et al*., 2012). Periventricular nodular heterotopia (PNH) is characterized by nodules of heterotopic grey matter located along the walls of the lateral ventricles and can usually be detected using MRI. PNH occurs either as an isolated malformation or in association with other brain abnormalities and is observed in a wide spectrum of anatomic and clinical presentations ranging from asymptomatic, small, unilateral or bilateral nodules, to extensive agglomerates of grey matter lining the lateral ventricles, in patients with severe epilepsy and intellectual disabilities (Sheen *et al*., 2004; Parrini *et al*., 2006).

To date, two genes, *FLNA* in Xq28 and *ARFGEF2* in 20q13.1 have been associated with X-linked bilateral PNH (Fox *et al*., 1998) and a rare autosomal recessive form of PNH with microcephaly, respectively (Sheen *et al*., 2004). *FLNA* codes for the F-actin binding cytoplasmic cross-linking phosphoprotein filamin A (FLNA) (Stossel *et al*., 2001). Filamin homologues are involved in regulation of cell stability and filopodial protrusion and motility across various biological systems (van der Flier and Sonnenberg, 2001). The mouse filamin A orthologue is abundantly expressed in the cell soma and leading processes of migratory neurons, and is widely distributed across the cortex, reaching the highest levels in the ventricular zone and within the cortex during neurogenesis (Guerrini and Parrini, 2010). *ARFGEF2* codes for the protein brefeldin A inhibited GEF2 (BIG2), which physically binds and interacts with FLNA and is involved in neuronal proliferation and migration (Sheen, 2012). As both FLNA and BIG2 are implicated in vesicle trafficking, it has been proposed that an overriding defect in the vesicle trafficking machinery may contribute to PNH formation (Sheen, 2012).

PNH has also been associated with fragile X syndrome (Moro *et al*., 2006), Williams syndrome (Ferland *et al*., 2006), 22q11 microdeletion syndrome (van Kogelenberg *et al*., 2010), duplications at 5p15 (Sheen *et al*., 2003), deletions at 1p36 (Neal *et al*., 2006), 5q14.3-q15 (Cardoso *et al*., 2009), 6p25 (Cellini *et al*., 2012) and 6q terminal deletion syndrome (Bertini *et al*., 2006; Dobyns *et al*., 2008), suggesting that additional causative genes are scattered throughout the genome. Using a comparative genomic hybridization (array-CGH) approach, we identified 12 patients (eight sporadic, one mother to son and one father to daughter transmission) exhibiting abnormal brain development with PNH, harbouring partially overlapping deletions of different extent in 6q25-qter and sharing a common 1.2 Mb minimal critical deletion in 6q27. Using whole-exome sequencing, we identified an additional patient with isolated bilateral PNH and epilepsy harbouring a *de novo* missense mutation in *C6orf70*, a gene mapping in the 6q27 minimal critical deleted region and encoding for a putative vesicular protein. Using *in utero* electroporation, we demonstrated that knocking down *C6orf70* expression causes neuronal migration defects in rodents. We suggest that haploinsufficiency or mutations of *C6orf70* are the main cause of the brain malformation complex with PNH observed in these patients.

Subjects and methods

Subjects

To discover genetic determinants for brain malformations, we analysed array-CGH on 155 patients with brain malformations, with or without associated epilepsy, intellectual disability and facial dysmorphisms. Brain malformations, occurring as either isolated defects or in various combinations, included lissencephaly, polymicrogyria, PNH, corpus callosum dysgenesis, cerebellar hypoplasia and other, minor abnormalities. Before performing array-CGH, we excluded mutations in the main known causative genes for the above malformations, including *FLNA*, *LIS1*, *DCX*, *ARX*, *TUBA1A* and *TUBB2B*, by direct sequencing or high resolution melting.

The above cohort included 84 patients with isolated PNH in whom CGH array was normal. Amongst them we selected 14 for whole exome sequencing and 50 for *C6orf70* mutation screening.

Blood samples were obtained from patients and their relatives after informed consent, according to the guidelines of the Human Research Ethics Committees of the participating institutions. Genomic DNA was extracted from blood leucocytes using an automated DNA isolation robot, according to the manufacturer's protocol (QIASymphony, Qiagen).

Array-comparative genomic hybridization analysis

Array-CGH analysis was performed in all 155 patients using a microarray kit (Human Genome CGH Microarray Kit 244 A; Agilent Technologies). Labelling and hybridization were performed following the manufacturer's protocols. Briefly, 500 ng purified DNA from a patient and a control (Promega Corporation) were double-digested with RsaI and AluI for 2 h at 37°C. After 20 min at 65°C, DNA of each digested sample was labelled by random priming (Invitrogen) for 2 h using Cy5-dUTP for the patient DNA and Cy3-dUTP for the control DNA. Labelled products were column-purified and prepared according to the manufacturer's protocol. After probe denaturation and pre-annealing with 50 mg Cot-1 DNA, hybridization was performed at 65°C with rotation for 40 h. After two washing steps, the arrays were analysed with the Agilent scanner and Feature Extraction software (V.9.1.3.1). A graphical overview was obtained using CGH analytics software (V.3.4.27).

Exome capture, next generation sequencing and mapping

Exomes were captured using the 38 Mb SureSelect^{TM} Exon Target Enrichment System (Agilent Technologies), as previously described (Xu *et al*., 2011). Briefly, 5 μg DNA was sheared producing fragments that were ~150–200 base pairs in size. A Klenow DNA polymerase (New England Biolabs) was employed for blunt end repair, followed by polyadenylation of 3′ ends. We then ligated pair-end adapters onto the DNA and amplified the library with Herculase II (Agilent Technologies) polymerase (4–6 cycles). Following quality control assessment (Agilent Bioanalyzer, Agilent Technologies) we proceeded with hybridization (24 h at 65°C). A post-hybridization amplification step using Herculase II polymerase followed (10–12 cycles), before loading the capture libraries (10 nM) onto an Illumina flowcell for 51 nucleotide paired-end sequencing on an Illumina GAIIx machine (Illumina). The 51 bp paired-end reads were mapped using Stampy (Lunter and Goodson, 2011) and duplicate PCR reads removed using Picard. Single nucleotide polymorphisms and insertion or deletion of bases (indels) were identified employing an in-house algorithm, Platypus (Pagnamenta *et al*., 2012), followed by filtering of synonymous variants and those observed at an allele frequency <5%. Comparison with parental exomes permitted the identification of *de novo* variants that were confirmed by Sanger sequencing.

C6orf70 mutation screening

C6orf70 mutation screening was performed in 50 patients with sporadic isolated bilateral PNH. For each patient, we analysed the 18 coding exons and the flanking intronic regions corresponding to the complete *C6orf70* coding sequence reported in the UCSC database (RefSeq NM_018341.1). PCR reactions were performed with primers designed using Primer3 plus software. Genomic DNA template (50 ng) was amplified using FastStart Taq DNA Polymerase (Roche). PCR products were checked by 1.5% agarose gel electrophoresis, purified using ExoSAP-IT® (USB) and then analysed by direct sequencing, on both strands, using the BigDye® Terminator V1.1 chemistry (Life Technologies), on ABI Prism 3130XL automated capillary sequencer (Life Technologies). Primers used for *C6orf70* mutation screening are available upon request.

Complementary DNA preparation

Total RNA was isolated from rat whole brains at different developmental stages and from C6 rat glioma cells using the RNeasy Plus Mini Kit (Qiagen), according to the manufacturer's protocol. For RT-PCR and expression studies in human brains, we used Human Foetal Brain and Human Adult Brain Total RNAs from Clontech. Complementary DNA was synthesized using the Quantitect® Reverse Transcription Kit (Qiagen), according to the manufacturer's protocol.

Quantitative reverse transcriptase polymerase chain reaction

Quantitative RT-PCR was performed using oligonucleotides specific for both the human and rat 6q27 candidate genes (*THBS2*, *WDR27*, *PHF10*, *TCTE3*, *C6orf70* and *DLL1*), designed using the ProbeFinder online software. Amplification was carried out using SYBR Green chemistry (Roche) and Roche amplification technology (Light Cycler 480), using Cyclophilin A and GAPDH as control probes for rat and human samples, respectively. All experiments were performed in triplicate. Primers used for quantitative PCR are available upon request.

C6orf70 RT polymerase chain reaction

RT-PCR was performed using a set of primers designed to amplify overlapping fragments spanning all 18 exons of the canonical *C6orf70* isoform (NCBI accession number NM_018341.1). PCRs were performed using a 9800 fast thermal cycler (Life Technologies) with an annealing temperature of 58°C. PCR products were analysed on 1.2% agarose gel and bands corresponding to different PCR products were extracted from gel using the Nucleospin Extract II Kit (Macherey-Nagel). RT-PCR products isolated from gel were then cloned using the TOPO TA cloning Kit (Life Technologies), cycle sequenced using the BigDye® Terminator v.1.1 chemistry (Life Technologies) and analysed on ABI Prism 3130XL automated capillary sequencer (Life Technologies). Primers used for RT-PCR are available upon request.

RNA interference constructs

RNA interference experiments were performed using different short hairpin RNAs targeting the coding sequences of the 6q27 candidate genes: Dll1-shCDS2, target sequence: 5′-CAGGGCCGCTACTGCGATGAAT-3′; Phf10-shCDS4, target sequence: 5′-GACAGCTCCTCAGGCAATGTGT-3′; C6orf70-shCDS1, target sequence: 5′-GCCATCTCCCTCAGCGTGATGAA-3′ and C6orf70-shCDS2, target sequence: 5′-GCCTGCGAGTGCCTGCGCTATAA-3′. For *C6orf70*, we also generated, as a control, a non-targeting short hairpin RNA (C6orf70-shCDS2mis), with the similar nucleotide sequence to C6orf70-shCDS2 except in three nucleotides positions (target sequence: 5′-GCCTCCGAGTGGCTGGGCTATAA-3′). Short hairpin RNAs specificity was confirmed by BLAST search performed against databases. Annealed oligonucleotides were cloned into a mU6-pro vector (Yu *et al.*, 2002).

In utero electroporation

Wistar rats (Janvier) were mated, maintained and used in the INMED animal facilities, in agreement with European Union and French legislation. Embryonic Day 15 timed pregnant rats (Day 0 was defined as the day of confirmation of sperm-positive vaginal plugs) were anaesthetized with ketamine and xylazine (0.1 and 0.01 mg per body weight, respectively). The uterine horns of the pregnant rats were exposed and a lateral ventricle of each embryo was injected through pulled glass capillaries and a microinjector (Picospritzer II) with 2 mg/ml Fast green (Sigma Aldrich) combined with the following DNA constructs: 0.5 μg/μl pCAGGS-red fluorescent protein (RFP) either alone or with 1.5 μg/μl of short hairpin RNA construct targeting the 6q27 candidate genes messenger RNAs. Plasmids were then electroporated by discharging 4000 μF capacitor charged to 50 V with a BTX ECM 830 electroporator (BTX Harvard apparatus). The voltage was discharged in five electric pulses at 950 ms intervals through 5 mm electrodes placed on the head of the embryo, across the uterine wall. *In utero* electroporation experiments were performed in embryonic day 15.5 (E15.5) rats, as this is a time coincident with tangential and radial migration of the newborn neurons to the cortex.

Quantitative analysis

Quantification was performed with either the eCELLence software (for C6orf70-shCDS2 RNA interference and rescue experiments) or the ImageJ plugin Cell Counter (for C6orf70-shCDS1 RNA interference experiments), on embryonic Day 20 coronal sections (100 μm) located in the dorso-lateral neocortex. Relative positions of transfected cells were estimated by counting RFP-positive cells in eight areas of interest, normalized in individual sections, to fit within the whole thickness of the cortex. These areas were divided in three main regions, corresponding to the ventricular zone (strata 1 and 2), the intermediate zone (strata 3–5) and the cortical plate (strata 6–8).

Cells culture and transfection

C6 rat glioma and Human Embryonic Kidney 293T cells (HEK293T) cells were maintained at 37°C in a humidified 5% CO_2 incubator in Dulbecco's modified Eagle's medium (Invitrogen) supplemented with 10% foetal bovine serum (Invitrogen), 1 mM L-glutamine and D-glucose. C6 rat glioma cells were transfected with short hairpin RNAs targeting the coding sequence of *C6orf70*, whereas HEK293T cells were transfected with myc-tagged wild-type or mutant *C6orf70* constructs. All the transfections were performed using the Neon® Transfection System (Invitrogen) according to the manufacturer's protocol.

Immunocytochemistry

HEK293T cells were fixed in antigenfix (Diapath), for 15 min and blocked at room temperature for 1 h with 5% normal goat serum, 0.3% Triton X-100 in PBS and incubated overnight at 4°C with a set of antibodies against GM130 (1/1000, BD biosciences), KDEL (1/400, Stressgen), EEA1 (1/500, BD biosciences), LAMP1 (1/200, Biolegend) and anti-myc (1/300, Bethyl lab). Sections were imaged on a laser-scanning confocal microscope (FluoView 300; Olympus and TCS SP5 X Leica).

Western blot analysis

HEK293T cells were lysed in Lysis buffer (150 mM NaCl, 50 mM Tris–HCl, pH 8.0, 50 mM NaF, 0.5% Nonidet P40, 2 mM EDTA, protease inhibitor cocktail) at 4°C. Proteins were then heat-denatured, processed by SDS–PAGE, transferred to nitrocellulose and immunoblotted with the following primary antibodies: anti-α-tubulin (1/10000, Sigma Aldrich) and anti-myc (1/1000, Bethyl lab). The proteins were detected with the Western Lumi-Light Kit chemiluminescence reagent (GE Healthcare).

Statistical data

Statistical analysis was performed with GraphPad Prism software. A two-sample Student's *t*-test was used to compare means of two independent groups if the distribution of the data was normal. When the normality test failed, the non-parametric Mann Whitney test was used. The one-way ANOVA all-Tukey test was used to compare multiple groups.

For the immunocytochemistry experiments, contingency was measured using the two-sided Fisher's exact test. For small samples, results were confirmed using two-sided Chi-square test. Values are represented as normalized values.

Results

Haploinsufficiency or mutations of *C6orf70* cause abnormal brain development with periventricular nodular heterotopia

We identified 12/155 patients (eight sporadic, one mother to son and one father to daughter transmission), harbouring partially overlapping deletions of different extent in 6q25-qter (Fig. 1A and Table 1). Patients exhibited a combination of developmental brain abnormalities variably including unilateral or bilateral, isolated or scattered nodules of PNH, with hypoplastic corpus callosum, colpocephaly, polymicrogyria, under-rotated and hypoplastic hippocampi and cerebellar hypoplasia (Fig. 2). These anatomical features were associated with a constellation of clinical manifestations including epilepsy (9/12), developmental delay (12/12), ataxic or clumsy gait (6/12) and facial dysmorphisms (11/12) (Table 1 and Supplementary Fig. 1).

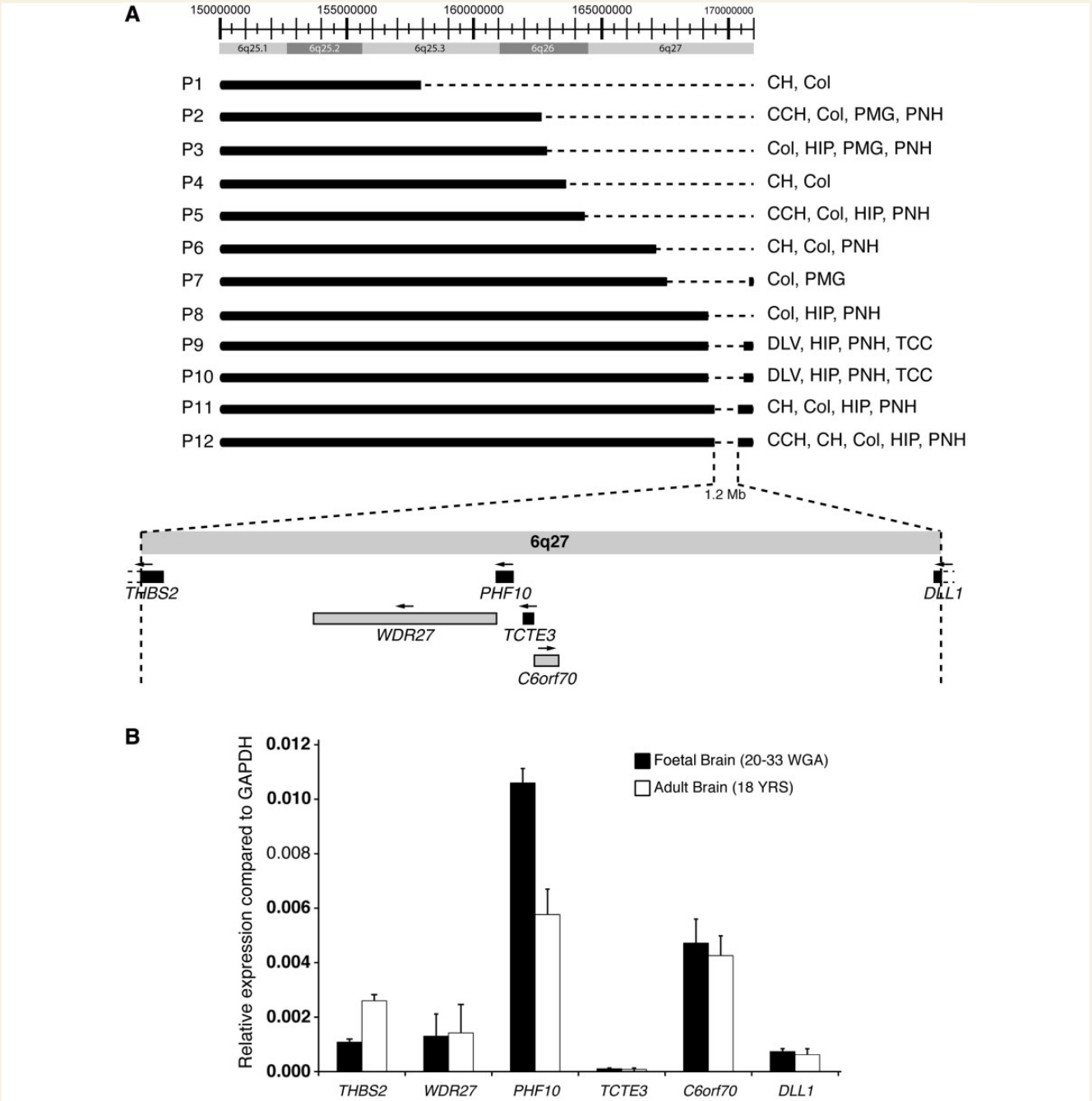

Figure 1 PNH critical region in 6q27 and expression of candidate genes in human brain. (**A**) Schematic representation of the extension of the deletions identified through array CGH analysis. Horizontal, dashed lines indicate the deleted genomic regions identified in patients and the observed brain malformations are indicated on the right side of the scheme. According to the UCSC hg17 assembly (May 2004), the 1.2 Mb minimal critical deleted region contains four known genes (*THBS2*, *PHF10*, *TCTE3* and *DLL1*, indicated by black boxes) and two predicted genes (*WDR27* and *C6orf70*, indicated by grey boxes). CCH = corpus callosum hypoplasia; CH = cerebellar hypoplasia; Col = colpocephaly; DLV = dilated lateral ventricles; HIP = under rotated hypoplastic hippocampi; PMG = polymicrogyria; PNH = periventricular nodular heterotopia; TCC = thin corpus callosum. (**B**) Quantitative RT-PCR revealing that the majority of the genes mapping in the 6q27 minimal critical deleted region are expressed in foetal and adult human brain. WGA = weeks of gestational age; YRS = years.

The minimal critical deleted region shared by all patients spans an interval of ~1.2 Mb in 6q27 (Fig. 1A). Bioinformatics analysis revealed that this interval contains four known genes (*THBS2*, *PHF10*, *TCTE3* and *DLL1*) and two predicted genes (*WDR27* and *C6orf70*) (Fig. 1A). Thrombospondin-2 (*THBS2*) is an adhesive glycoprotein that mediates cell-to-cell and cell-to-matrix interactions. It is highly expressed in intervertebral disk tissue and it has been hypothesized that mutations in this gene may be

Table 1 Summary of clinical features in patients harbouring a 6q27 deletion

Patient #	Sex	Age (years)	MRI features	Reason for first medical evaluation (age)	Epilepsy (onset)	Neurological examination	Other clinical features	Facial dysmorphisms
Patient 1	F	15	CH, Col	Hypotonia, moderate psychomotor delay (7 mths)	Focal - Occipital (5 yrs)	Hypotonia, strabismus, hypermetropia, dysmetria	Joint laxity	Depressed nasal root, low frontal hairline, hypertelorism, short palpebral fissures, micrognathia, high palate, low set ears
Patient 2	M	12.5	CCH, Col, left perisylvian PMG, bilateral PNH in temporal horns	Epilepsy, moderate psychomotor delay (1 yr)	Focal - CPS (1 yr)	Strabismus, mild hypotonia,	Joint laxity	Short neck, hypertelorism, bulbous nasal root, micrognathia, low set ears
Patient 3	M	13	Col, right HIP, PMG in right frontal lobe, unilateral PNH in left temporal horn	Feeding difficulties, mild psychomotor delay (3 mths)	Focal - occipital (18 mths)	Hypotonia, strabismus, hypermetropia, dysmetria	Hypospadias, phimosis, joint laxity	Short neck, low frontal hairline, flat nasal bridge, hypertelorism, short palpebral fissures, micrognathia, high palate, epicanthal folds
Patient 4	M	25	CH, Col	Moderate psychomotor delay (18 mths)	Focal - occipital, GTCS (16 yrs)	Hypotonia, strabismus, hypermetropia, nystagmus, dysmetria	Scoliosis, hyperkeratosis, obesity, gynecomastia	Macrocephaly, low frontal hairline, downslanting palpebral fissures, hypertelorism, dysmorphic cup shaped ears, broad philtrum, thick lips
Patient 5	F	7	CCH, Col, bilateral HIP, unilateral PNH in left temporal horn	Triventricular hydrocephalus (birth), moderate psychomotor delay	Isolated seizure (1 year)	Hypotonia, ataxic gait, dysmetry, hyperactivity	Talus valgus	Arched eyebrows, broad nasal bridge, bulbous nose, anteverted ears, thick lips, narrow and high palate
Patient 6	M	15	CH, Col, unilateral PNH in right temporal horn	Hypotonia, mild psychomotor delay (3 mths)	No	Hypotonia, strabismus, clumsy gait, slow ocular saccadic movements, nystagmus, dysmetria	Joint laxity, valgus first toes	Plagiocephaly, low frontal hairline, hypertelorism, epicanthal folds, downslanting palpebral fissures, short neck, prominent forehead, micrognathia, broad philtrum, thick lips
Patient 7	M	33	Col, right perisylvian PMG	Epilepsy, moderate psychomotor delay (15 mths)	FS, Focal - occipital (15 mths)	Strabismus, hypermetropia	Joint laxity	Broad nasal root, narrow palpebral fissures, large prominent ears, high palate, micrognathia
Patient 8	M	18	Col, right HIP, left unilateral PNH	Mild psychomotor delay (15 yrs)	Focal - CPS (Childhood)	Hypotonia, strabismus, ataxic gait, dysmetria	Scoliosis, 12th right rib agenesis	Hypertelorism, bulbous nose, short philtrum, retrognathia
Patient 9	M	43	Dilated lateral ventricles, bilateral HIP, bilateral PNH in temporal horns, TCC	Mild psychomotor delay	No	Clumsy gait	None	None
Patient 10 (Patient 9's daughter)	F	1.5	Dilated lateral ventricles, bilateral HIP, bilateral PNH in temporal horns, TCC	Prenatal diagnosis of ventriculomegaly by ultrasound at 20 weeks. Mild psychomotor delay	No	Normal, other than global delay	Wide-spaced nipples, dimples over shoulders and elbows	Prominent forehead, hypertelorism, epicanthal folds, downslanting palpebral fissures, small cupped low set ears, broad nasal root, broad philtrum, thick lips
Patient 11	F	25	CH, Col, right HIP, bilateral PNH in temporal horns	Mild psychomotor delay, behavioural problems	Focal - CPS (4 yrs)	Clumsy gait	Bilateral clinodactyly	Bulbous nose

(continued)

Table 1 Continued

Patient #	Sex	Age (years)	MRI features	Reason for first medical evaluation (age)	Epilepsy (onset)	Neurological examination	Other clinical features	Facial dysmorphisms
Patient 12 (Patient 11's son)	M	6	CCH, CH, Col, right HIP, bilateral PNH in temporal horns	Prenatal diagnosis of PNH by foetal MRI following colpocephaly diagnosed by ultrasound, later development of mild psychomotor delay, behavioural problems and epilepsy	Focal - CPS (16 mths)	Strabismus, clumsy gait	Bilateral clinodactyly	Dolicocephaly, prominent metopic suture and forehead, low set malrotated ears, bulbous nose, broad philtrum, thick lips
Patient 13	F	7	Bilateral PNH in frontal horns	Epilepsy, mild psychomotor delay (22 wks)	Infantile spasms (22 wks), then focal motor	Strabismus	Liver adenoma	None

CCH = corpus callosum hypoplasia; CH = cerebellar hypoplasia; Col = colpocephaly; CPS = complex partial seizures; FS = febrile seizures; GTCS = generalized tonic clonic seizures; HIP = under rotated hypoplastic hippocampi; PMG = polymicrogyria; TCC = thin corpus callosum.

associated with susceptibility to intervertebral disc disease (Hirose *et al.*, 2008). *WDR27* is predicted to code for a WD repeat-containing protein with unknown function. *PHF10* contains, according to the UniProt database, a predicted open reading frame that codes for a protein with two zinc finger domains. This gene belongs to the neural progenitors-specific chromatin-remodelling complex (npBAF complex) and is required for the proliferation of neural progenitors. *TCTE3* seems to be an accessory component of axonal dynein and cytoplasmic dynein 1. It is expressed predominantly in testis and may be involved in male sterility (Neesen *et al.*, 2002). *C6orf70* is predicted to code for a potential multi-pass membrane protein with unknown function. *DLL1* is a human homologue of the notch delta ligand and is a member of the delta/serrate/jagged family. It plays a role in mediating cell fate decisions during haematopoiesis and may play a role in cell-to-cell communication (Jaleco *et al.*, 2001). Quantitative RT-PCR analysis revealed that the majority of the genes mapping in the 6q27 minimal critical deleted region are widely expressed in human foetal and adult brains (Fig. 1B).

Whole exome sequencing in 14 patients with isolated bilateral PNH who did not harbour copy number variations identified one patient (Patient 13) with a *de novo* substitution (T > A) in the predicted *C6orf70* gene (Genbank accession number NM_018341.1), that causes the substitution of an isoleucine (Ile) with an asparagine (Asn) (Fig. 3A–D). The mutation was not described as a known variant in the Kaviar2 database. This patient, a female, was referred for developmental delay and seizures and was last assessed at the age of 36 months. She was born at term with a birth weight on 25th centile and head circumference on the 9th centile. Pregnancy, delivery and the neonatal period were uncomplicated. There was no family history of note. She developed infantile spasms with hypsarrhythmia at the age of 3 months and was treated with vigabatrin and prednisolone. Seizures were controlled from age 6 months for ~6 months and then relapsed. She sat unaided at 8 months and walked by 18 months. Speech was delayed. Laboratory investigations including array-CGH analysis and *FLNA, ARFGEF2, TSC1* and *TSC2* mutation screening were negative. The patient presented isolated bilateral PNH in the frontal horns (Fig. 2W).

We then investigated how common mutations in *C6orf70* are in 50 patients with isolated bilateral PNH. Mutation screening of all 18 exons of *C6orf70* gene did not reveal additional variants, suggesting that point mutations of this gene are not a frequent cause of isolated bilateral PNH.

To investigate whether haploinsufficiency of one of the genes mapping in 6q27 would cause the phenotype observed in patients harbouring the minimal critical deletion, we explored *in vivo* their role in brain development using the *in utero* RNA interference-mediated knockdown approach (Bai *et al.*, 2003; Carabalona *et al.*, 2012) to silence their expression in rat embryonic neuronal progenitors. We first examined the temporal expression of the candidate genes in the developing rat neocortex. Quantitative RT-PCR experiments, from embryonic Day 12 (E12) to postnatal Day 30 (P30), showed that three out of six candidate genes (*Phf10*, *C6orf70* and *Dll1*) are expressed in rat brain, although at different levels (Fig. 4A).

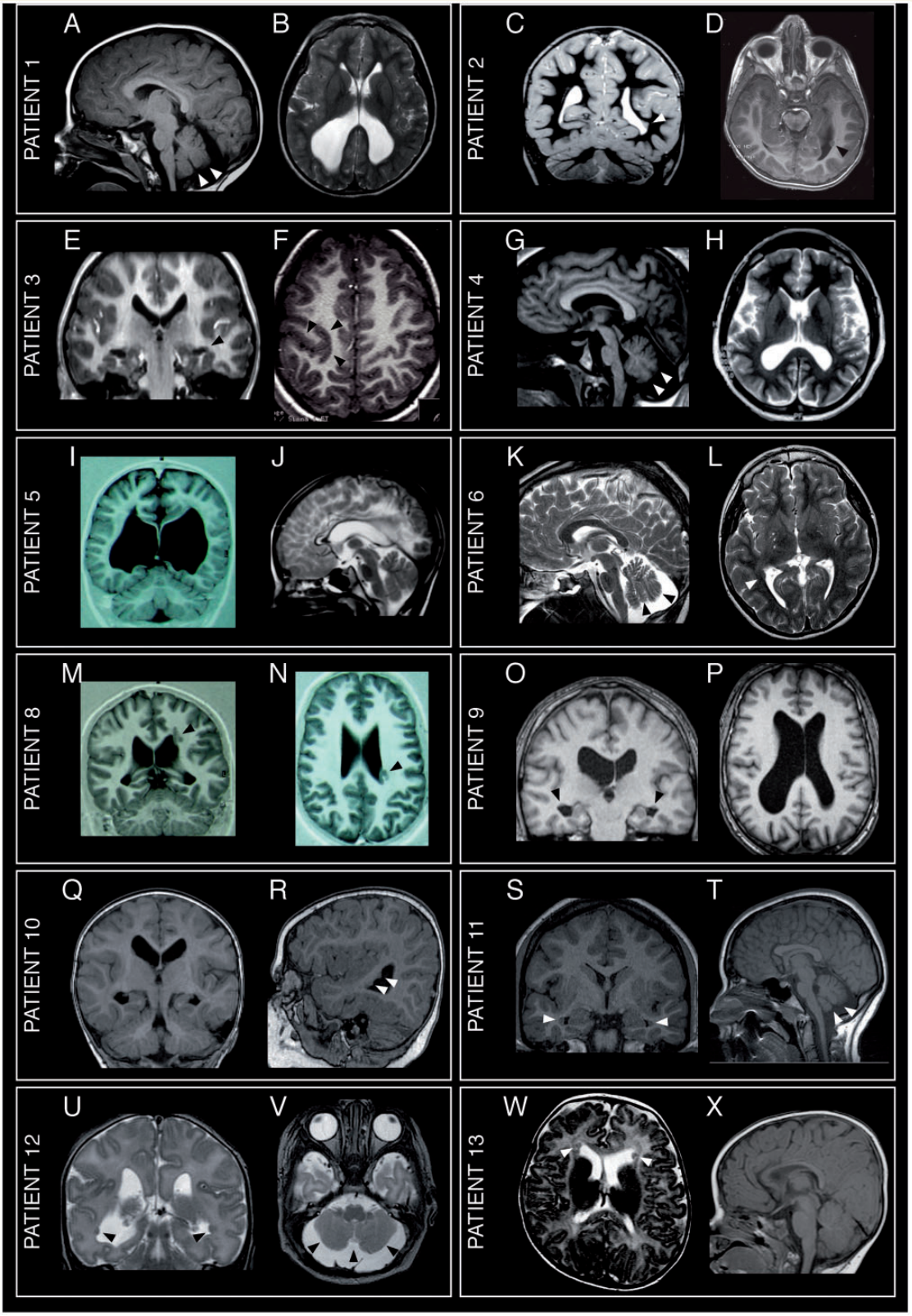

Figure 2 Brain MRI images summarizing the main anatomic features in 12 patients with 6q27 deletion and in one patient with *C6orf70* point mutation. Patient 1: (**A**) T_1-weighed sagittal section through the midline, showing cerebellar vermis hypoplasia (white arrowheads) with mega cisterna magna. (**B**) T_2-weighed axial section showing colpocephaly. Patient 2: (**C**) T_2-weighed coronal section showing infolding of the insular cortex on the left with underlying PNH (white arrowhead). (**D**) T_1-weighed axial section showing PNH protruding in the ventricular lumen (black arrowhead). Patient 3: (**E**) T_1-weighed coronal section showing dilated temporal horns with a small area of PNH on the left (black arrowhead). (**F**) T_1-weighed axial section showing abnormal thickening and sulcation in the premotor cortex on the

(continued)

We then generated different short hairpin RNAs targeting the coding sequences of these three genes. Short hairpin RNAs were introduced in combination with a RFP encoding reporter construct into neuronal progenitors in the rat neocortex by *in utero* electroporation at embryonic Day 15, when neurons committed to upper cortical layers are generated. Relative RFP-positive cells in the ventricular zone, intermediate zone, and cortical plate of the neocortex were examined 5 days later. *In utero* silencing of *Dll1* and *Phf10* resulted in a slight delay of radial neuronal migration (data not shown), whereas silencing of *C6orf70* resulted in a massive neuronal migration defect and in the development of heterotopic nodules along the walls of the lateral ventricles (Fig. 4B–E). In embryonic Day 20 control brain sections, the majority of RFP (90.2 + 2.1%; $n = 10$ embryos) or C6orf70-shCDS2mis (74.7 + 3.6%; $n = 7$ embryos) transfected cells reached the cortical plate (Fig. 4B, D and E). Conversely, transfection with C6orf70-shCDS2 induced a significant arrest of cells within the ventricular zone (Fig. 4C and E; 14.3 + 3.7%; $n = 8$ embryos; $P < 0.001$). We carried out similar experiments with C6orf70-shCDS1 construct ($n = 7$ embryos) and found it to lead to the same migration arrest, confirming the specificity of our results (Supplementary Fig. 2).

In vitro analysis in C6 rat glioma cells demonstrated that C6orf70-shCDS1, targeting the 5′ coding region of the gene (Supplementary Fig. 3A) and C6orf70-shCDS2, targeting the 3′ coding region of the gene (Supplementary Fig. 3A) repressed *C6orf70* expression by ~40–60%, whereas the control C6orf70-shCDS2mis did not destabilize the *C6orf70* messenger RNA (Supplementary Fig. 3B).

To validate *in utero* electroporation results, we performed a rescue experiment in which the C6orf70-shCDS2 was co-transfected with a plasmid encoding human C6orf70 (hC6orf70-IRES-GFP). Human and rat *C6orf70* nucleotide sequences do not match in the region targeted by the C6orf70-shCDS2 and therefore the human *C6orf70* is not susceptible to RNA interference. As expected, transfection with the human *C6orf70* overexpression construct alone did not alter neuronal migration, but prevented the migration arrest in the ventricular zone of cells co-transfected with the C6orf70-shCDS2 (Fig. 5; 1.8 + 0.6%, $n = 9$ embryos, $P < 0.001$). The C6orf70-shCDS2 induced phenotype is consequently due to specific knock-down of endogenous *C6orf70*.

Alternative splicing produces two C6orf70 protein isoforms

As *C6orf70* is a predicted gene, we analysed its genomic structure. The canonical *C6orf70* isoform, corresponding to the NCBI accession number NM_018341.1, consists of 18 exons, with the ATG codon in Exon 1. RT-PCR analysis, performed in human foetal brain, revealed different isoforms of the *C6orf70* messenger RNA, with possible exon skipping involving exons 2, 3 and 4 and the possible retention of introns 2, 3 and 4 (Supplementary Fig. 4). *In silico* analysis of the different *C6orf70* isoforms, performed using the software ORF Finder, revealed that a protein of 552 amino acids may be obtained with the usage of an alternative ATG in the exon 4 of the *C6orf70* canonical sequence and that a protein of 509 amino acids may be obtained with the usage of an alternative ATG in the exon 6. These proteins are predicted to contain two transmembrane domains (Fig. 3E and F). The mutation identified in Patient 13 affects both isoforms (corresponding to c.752T > A; p.Ile250Asn in the long isoform and c.622T > A; p.Ile207Asn in the short isoform). *In silico* predictions also revealed that the mutation, which causes the substitution of a non-polar hydrophobic amino acid (Ile) with a polar negative one (Asn), occurred in an evolutionarily conserved residue (Fig. 3D).

p.Ile250Asn-p.Ile207Asn mutation affects C6orf70 protein stability and subcellular organization

To evaluate the effects of the mutation identified in Patient 13, we performed transient transfections of HEK-293T cells with full-length myc-tagged C6orf70-wild-type or p.Ile250Asn-p.Ile207Asn mutant constructs, evaluating protein levels by western blot with an anti-myc antibody. In both cases, we obtained two bands corresponding to proteins of expected size of ~64 and 56 kDa, respectively (Fig. 6A). However, the overall expression level of the mutant C6orf70 was markedly reduced in comparison

Figure 2 Continued
right (black arrowheads). Patient 4: (**G**) T_2-weighed sagittal section through the midline, showing cerebellar hypoplasia (white arrowheads) with mega cisterna magna. (**H**) T_2-weighed axial section showing colpocephaly. Patient 5: (**I**) T_1-weighed coronal section showing severe colpocephaly. (**J**) T_2-weighed sagittal section through the midline, showing corpus callosum hypoplasia. Patient 6: (**K**) T_2-weighed sagittal section through the midline, showing cerebellar vermis hypoplasia (black arrowheads) with mega cisterna magna. (**L**) T_2-weighed axial section showing mild colpocephaly with unilateral PNH (white arrowheads). Patient 8: (**M**) T_1-weighed coronal section showing colpocephaly with unilateral PNH (black arrowhead). (**N**) T_2-weighed axial section showing PNH protruding into the left lateral ventricle. Patient 9: (**O**) T_1-weighed coronal section showing asymmetric lateral ventricles, under-rotated hippocampi and small areas of PNH along the margins of the temporal horns (black arrowheads). (**P**) T_1-weighed axial section showing dilated ventricles with colpocephaly. Patient 10 (Patient's 9 daughter): (**Q**) T_1-weighed coronal section showing under rotated hippocampi. (**R**) T_1-weighed sagittal image showing PNH in the temporal horns (white arrowheads). Patient 11: (**S**) T_1-weighed coronal section showing bilateral PNH along the walls of the temporal horns of the lateral ventricles (white arrowheads). (**T**) T_1-weighed sagittal section through the midline, showing cerebellar vermis hypoplasia with mega cisterna magna. Patient 12 (Patient's 11 son): both images are T_2-weighed. (**U**) Coronal section showing bilateral PNH (black arrowheads) and dilated ventricles. (**V**) Axial image showing cerebellar hypoplasia (black arrowheads). Patient 13: (**W**) T_2-weighed axial section showing bilateral PNH in the frontal horns (white arrowheads). (**X**) T_1-weighed sagittal section through the midline, showing normal cerebellum and corpus callosum.

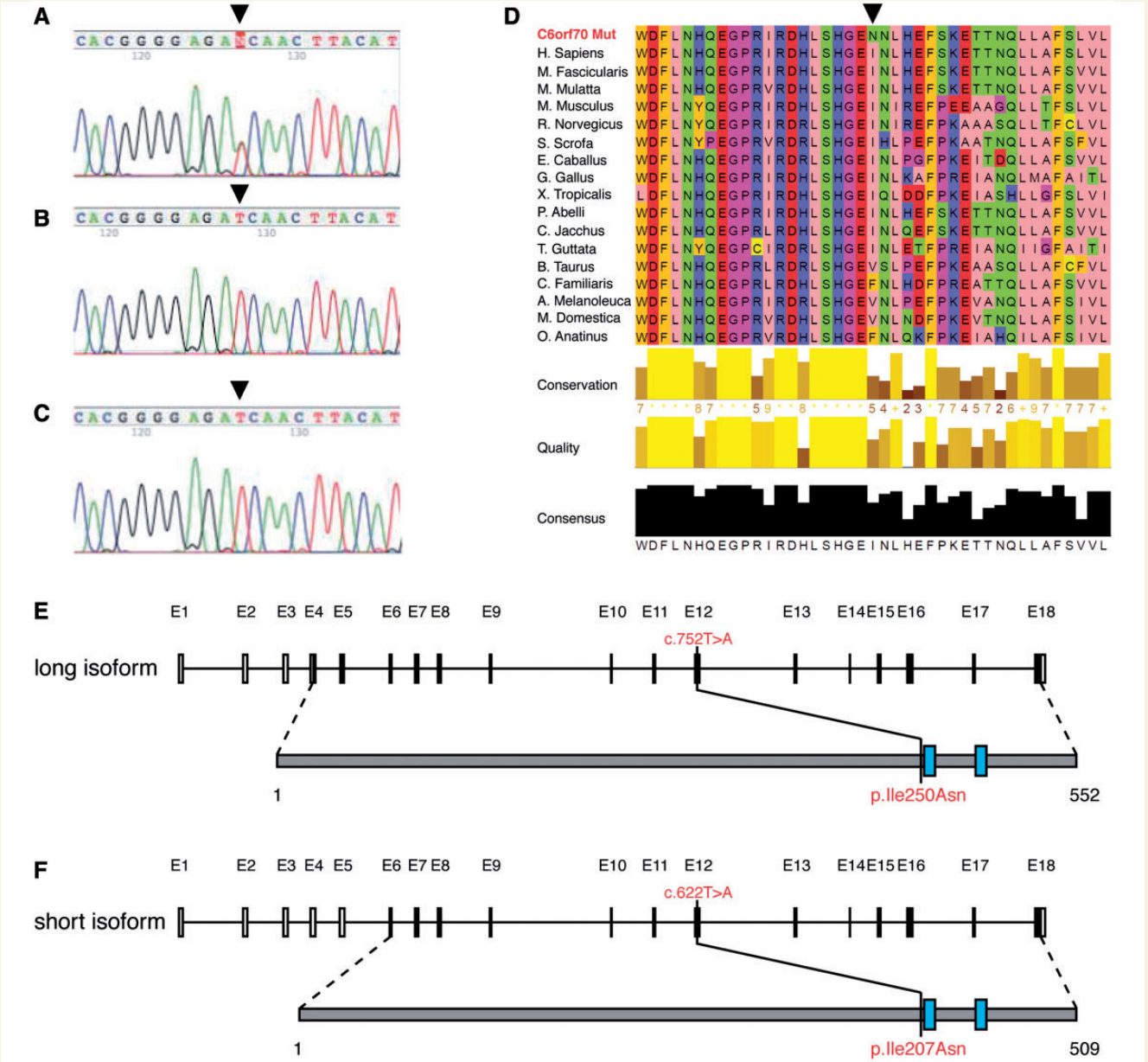

Figure 3 *In silico* characterization of *C6orf70* missense mutation identified in Patient 13. Sanger sequencing showing that the mutation occurred *de novo* (**A**) proband, (**B**) father, (**C**) mother. The T > A mutation causes an isoleucine to asparagine substitution. (**D**) *In silico* multiple sequence alignment, performed using Jalview software, reveals that the mutation occurred in an amino acid that is conserved among the species and that, according to the physicochemical properties of the wild-type and mutant amino acid, the mutation resulted in the substitution of a non-polar hydrophobic amino acid (isoleucine, I, coloured in pink) with a polar, negative one (asparagine, N, coloured in green). Black arrowheads indicate the position of the mutation (**A**–**C**) and of the mutated amino acid (**D**). (**E** and **F**) Schematic representation of the two C6orf70 protein isoforms identified in the brain. *In silico* predictions performed using ORF Finder reveals that the different messenger RNA isoforms identified through RT-PCR in human foetal brain (see Supplementary Fig. 4) are translated in two different protein isoforms consisting of 552 amino acids (long isoform) (**E**) and 509 amino acids (short isoform) (**F**), respectively. The missense mutation identified in Patient 13 affects both messenger RNA isoforms. White boxes: non-coding exons, black boxes: coding exons, grey boxes: predicted proteins, cyan boxes: predicted transmembrane domains within the proteins. Exons are numbered in the top of each panel according to the canonical *C6orf70* isoform, corresponding to the NCBI accession number NM_018341.1.

with wild-type (~58% of reduction for the 64 kDa isoform and 12% of reduction for the 56 kDa isoform, Fig. 6A and B), suggesting a pathogenic role.

We then used confocal microscopy to determine the subcellular localization of the C6orf70 wild-type and mutant proteins. Immunocytochemistry revealed that, while in cells transfected with myc-tagged wild-type construct C6orf70 was distributed in a puncta-like pattern (Fig. 6C and E, 77 cells analysed: 46 cells with a puncta-like distribution, 31 cells with a diffuse pattern distribution), transfection with the mutant construct generated a

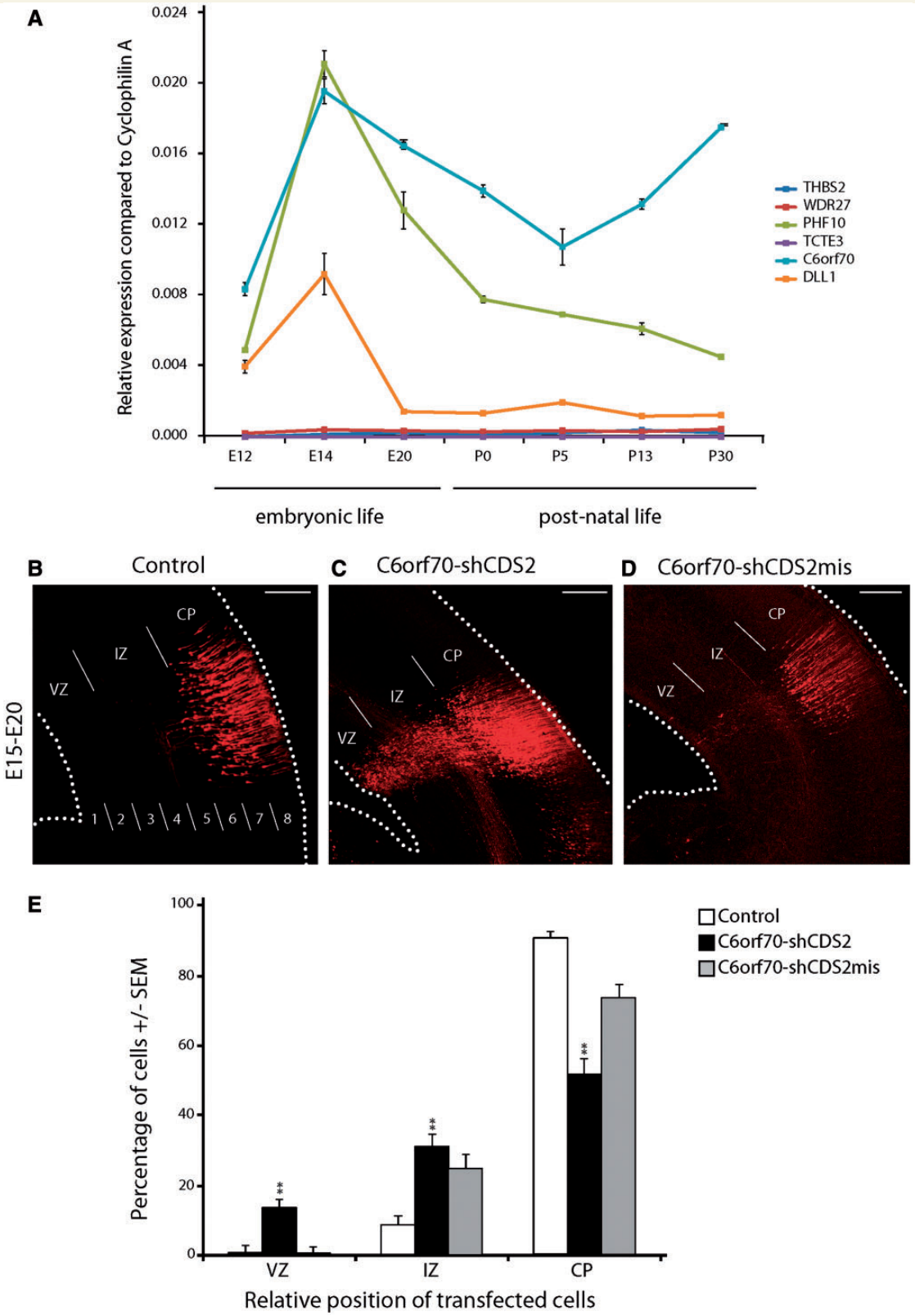

Figure 4 *Phf10*, *C6orf70* and *Dll1* genes are expressed in the developing rat neocortex and *in utero* knockdown of *C6orf70* expression alters radial neuronal migration. (**A**) Quantitative RT-PCR analysis revealed that three out of six genes mapping in 6q27 (*Phf10*, *C6orf70* and *Dll1*) are expressed in brain at different time points, with a peak at embryonic Day 14 (E14), corresponding to the neuronal migration process. Cyclophilin A was used for normalization. (**B–D**) Representative neocortical coronal sections showing migration of transfected cells 5 days after electroporation at embryonic Day 15 (E15) with either RFP construct alone (control) (**B**) or in combination with short

(continued)

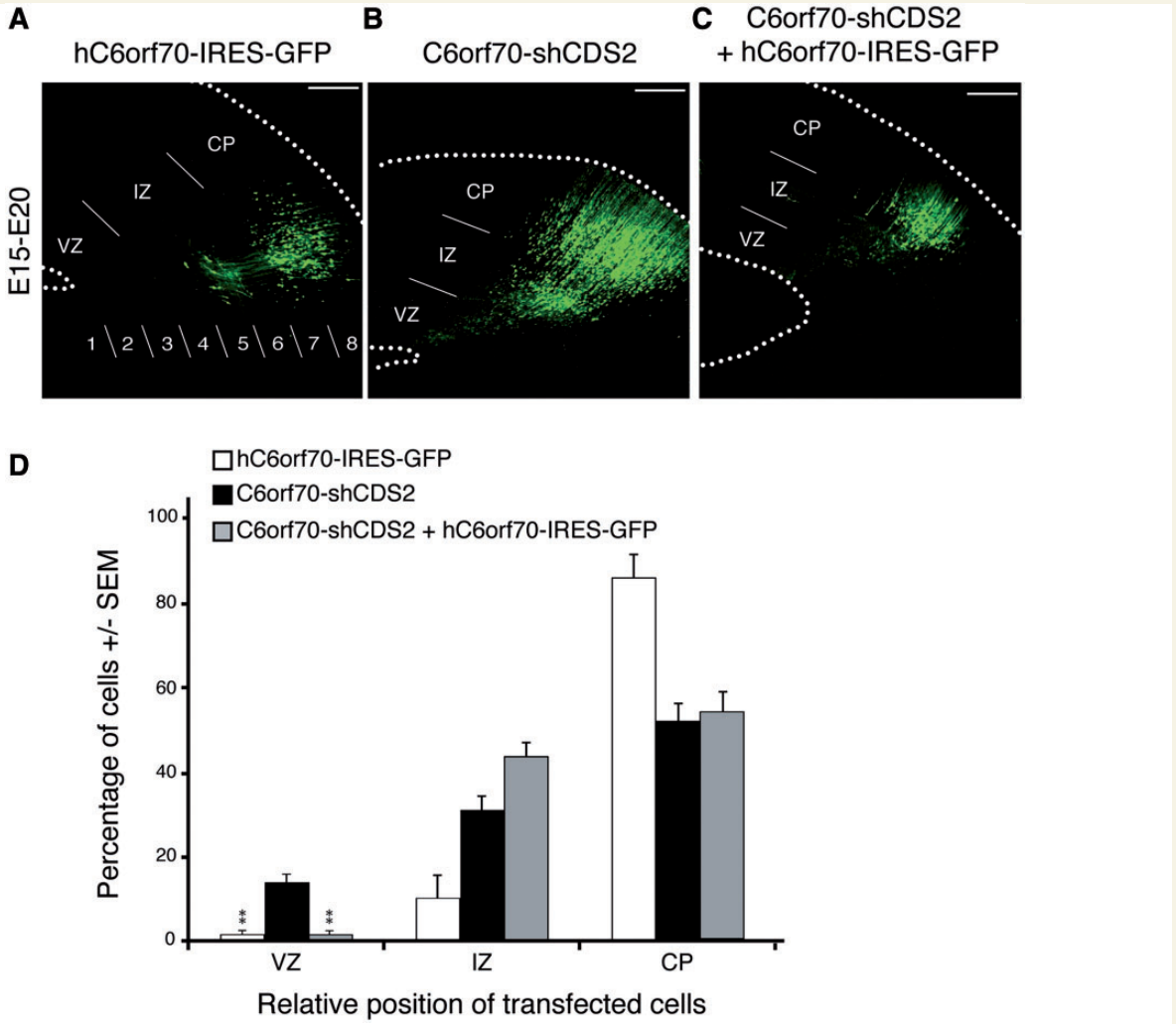

Figure 5 Expression of the human *C6orf70* complementary DNA rescues the radial migration defect of C6orf70-knockdown cortical neurons. (**A–C**) Representative coronal sections of embryonic Day 20 (E20) rat brains 5 days after electroporation with hC6orf70-IRES-GFP construct (**A**), C6orf70-shCDS2 combined with pGAGIG empty plasmid (**B**), or with hC6orf70-IRES-GFP (**C**) revealed that, as expected, overexpression of human *C6orf70* did not alter migration (**A**), but prevented the migration arrest in the ventricular zone (VZ) of cells co-transfected with the C6orf70-shCDS2 (**C**). Quantification (means + SEM) of GFP-positive cell distribution in the ventricular zone (strata 1, 2), the intermediate zone (IZ, strata 3–5) and the cortical plate (CP, strata 6–8) of embryonic Day 20 (E20) independent brains [hC6orf70-IRES-GFP ($n = 5$); C6orf70-shCDS2 ($n = 9$) or hC6orf70-IRES-GFP combined with C6orf70-shCDS2 ($n = 7$)] and expressed as a percentage of the total (**D**). $^{**}P < 0.001$.

Figure 4 Continued
hairpin RNA targeting the *C6orf70* coding sequence (C6orf70-shCDS2) (**C**) or with the mismatch construct (C6orf70-shCDS2mis) (**D**). As expected, the electroporation with the control and mismatch constructs did not impair neuronal migration (**B** and **D**), whereas the transfection with the C6orf70-shCDS2 induced a significant arrest of cells within the ventricular zone (VZ) (**C**). (**E**) Quantification (means + SEM) of RFP-positive cell distribution in eight arbitrary strata dividing the cortex. RFP-positive cells were counted in strata 1 and 2 corresponding to the ventricular zone, in strata 3, 4 and 5 to the intermediate zone (IZ) and strata 6, 7 and 8 to the cortical plate (CP) and expressed as a percentage of the total. At embryonic Day 20 (E20), the majority of RFP (90.2 + 2.1%; $n = 10$ embryos) or C6orf70-shCDS2mism (74.7 + 3.6%; $n = 7$ embryos) transfected cells reached the cortical plate. Conversely, the transfection with C6orf70-shCDS2 induced a significant arrest of cells within the ventricular zone (**C** and **E**; 14.3 + 3.7%; $n = 8$ embryos;). $^{**}P < 0.001$ when compared with control. Scale bars = 200 μm.

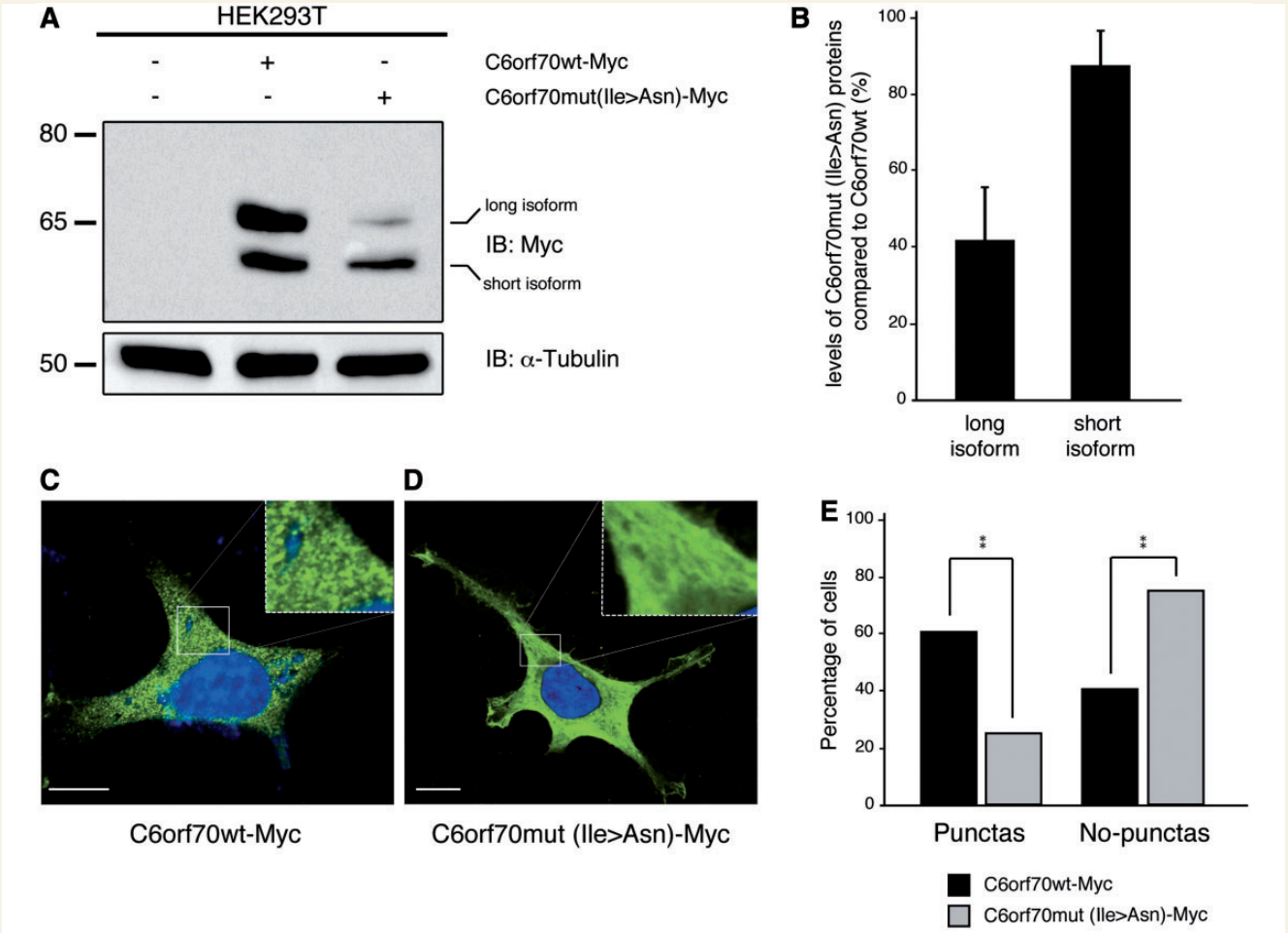

Figure 6 The mutation identified in Patient 13 affects C6orf70 protein stability and subcellular organization. (**A**) Western blot analysis performed on lysates obtained from HEK293T cells transfected with myc-tagged wild-type or p.Ile250Asn-p.Ile207Asn mutant *C6orf70* constructs reveals that the C6orf70 protein exists in human brain in two different isoforms of ~64 and 56 kDa. The total amount of the mutant proteins is reduced with respect to the wild-type (**A**, **B**). (**C**) Immunocytochemistry analysis shows that, in cells transfected with myc-tagged wild-type construct, C6orf70 proteins were distributed in a puncta-like pattern, whereas the transfection with the p.Ile250Asn-p.Ile207Asn mutant construct resulted predominantly in a dispersed pattern of staining (**D**). (**E**) Statistical analysis revealed a significant (**$P < 0.001$) switching from puncta-like to diffuse pattern of staining due to p.Ile250Asn-p.Ile207Asn mutation (Fisher exact test). Scale bars = 10 μm (**C** and **D**).

predominantly dispersed pattern of staining (Fig. 6D and E, 32 cells analysed: eight cells with a *puncta*-like distribution, 24 cells with a diffuse pattern distribution), suggesting that the p.Ile250Asn-p.Ile207Asn mutation also alters the subcellular distribution of C6orf70 proteins.

C6orf70 is a putative vesicular protein

As *puncta* are thought to reflect cytoplasmic vesicles (Schwarz-Romond *et al.*, 2005), and C6orf70 proteins have two predicted transmembrane domains, we investigated the possible association of C6orf70 proteins with membranous organelles *in vitro*. We co-stained cells transfected with myc-tagged wild-type *C6orf70* with antibodies against markers for Golgi apparatus (GM130), endoplasmic reticulum (KDEL), early endosomes (EEA1) and for late endosomes and lysosomes (LAMP1) (Fig. 7). Our data showed that myc-tagged C6orf70 puncta are mainly colocalized with the endoplasmic reticulum, but not with Golgi apparatus, early or late endosomes and lysosomes (Fig. 7).

Discussion

Different, rare chromosomal rearrangements have been associated with PNH but causative genes remain unknown (Guerrini and Parrini, 2010; van Kogelenberg *et al.*, 2010). Subtelomeric deletions in 6q26-qter have been associated with the 6q terminal deletion syndrome, featuring a range of developmental brain abnormalities including hydrocephalus, corpus callosum and cerebellar vermis dysgenesis, colpocephaly, polymicrogyria (Stevenson *et al.*, 2004; Eash *et al.*, 2005; Elia *et al.*, 2006; Striano *et al.*, 2006), and PNH (Bertini *et al.*, 2006; Dobyns *et al.*, 2008). Intellectual disability, epilepsy and dysmorphic features are present in most patients (Backx *et al.*, 2010; Gerber *et al.*, 2011).

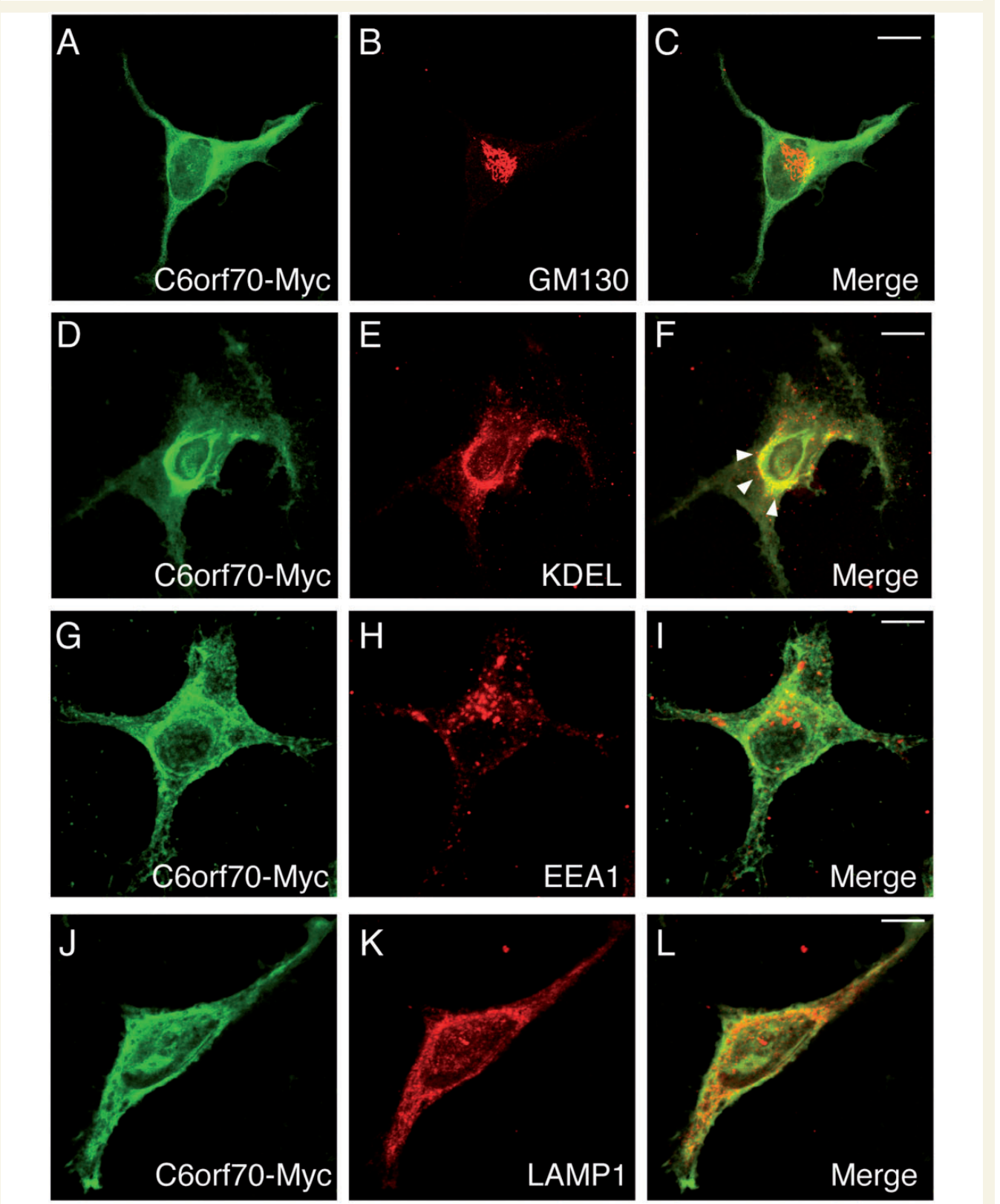

Figure 7 C6orf70 is a putative vesicle-associated protein. (**A–L**) Immunocytochemistry co-staining performed in HEK293T cells transfected with myc-tagged wild-type construct using antibodies against specific markers for Golgi apparatus (GM130) (**A–C**), endoplasmic reticulum (KDEL) (**D–F**), early endosomes (EEA1) (**G–I**) and late endosomes and lysosomes (LAMP1) (**J–L**), revealed a co-localization of myc-tagged *C6orf70* only with the endoplasmic reticulum (white arrowheads). Scale bars = 10 μm.

Considering the relative phenotypic heterogeneity, genetic diagnosis is usually made only after a deletion in 6q26-qter is identified.

In our series epilepsy, present in 9 of 12 patients with 6q25-qter deletion, was a main clinical feature. Developmental delay, with clumsy or ataxic gait was present in all patients and was often the reason for the first referral. Brain MRI revealed a range of developmental abnormalities, with PNH being the most consistent, although not universal, finding occurring in 9 out of 12 patients. Previous reports of patients with 6q26-qter deletions, as well as this study, might have under-reported PNH, likely due to the limitations of low resolution MRI in identifying isolated or scattered nodules that, especially in presence of severe colpocephaly, may be overlooked or misdiagnosed as a ventricular dimple caused by the depth of a sulcus. It is much easier to visualize the contiguous bilateral nodules observed, for example, in patients with *FLNA* gene mutations (Parrini *et al*., 2006) or in other major forms of bilateral PNH (Pisano *et al*., 2012). Other malformations observed in the series presented here included colpocephaly, occurring in 12 patients, corpus callosum dysgenesis and cerebellar hypoplasia, occurring in five patients each, and polymicrogyria occurring in three. Under rotated and hypoplastic hippocampi were observed in seven patients all having dilated temporal horns (Fig. 2). We could not identify a clear gradient of malformation severity from smaller to larger deletions, with the exception of polymicrogyria, which only occurred in patients with deletions >2 Mb (identified in Patient 8). It is possible that genes mapping to the larger deleted genomic regions contribute to phenotype variability.

We demonstrated that the minimal critical deleted region in 6q27 contains three genes that are expressed in human as well as rodent brain. Silencing *Phf10* and *Dll1*, through *in utero* electroporation, only caused slightly delayed neuronal migration, while silencing *C6orf70* reproduced PNH, suggesting that this gene plays a major role in the control of neuronal migration. This hypothesis was supported by the finding of a p.Ile250Asn-p.Ile207Asn mutation in a patient with isolated bilateral PNH and epilepsy.

C6orf70 is expressed in human and rodent developing brain, codes for a protein containing two transmembrane domains and is involved in neuronal migration. Both its puncta-like subcellular pattern of expression and its colocalization pattern with endoplasmic reticulum are consistent with the hypothesis of its being a putative vesicle-associated protein. Defects in the vesicle trafficking machinery are known to contribute to PNH formation, causing changes in the localization and stability of molecules associated with neuronal migration (Sheen, 2012). Indeed, FLNA dynamically associates with the Golgi apparatus and regulates the trafficking of membrane proteins (Liu *et al*., 1997; Sverdlov *et al*., 2009) and ARFGEF2 is required for vesicle and membrane trafficking from the trans-Golgi network (Shin *et al*., 2005). Therefore, we can hypothesize that vesicle trafficking machinery impairment may be the causative pathogenic mechanism underlying PNH also in patients harbouring 6q27 chromosomal deletions or mutations in *C6orf70*. Further studies will be necessary to investigate the role of *C6orf70* in vesicle trafficking and unravel the molecular pathways affected by mutations in this gene.

As mutation screening of *C6orf70* in 50 patients with isolated bilateral PNH did not reveal additional variants, it is likely that point mutations of this gene are an infrequent cause of such a neuronal migration defect when it occurs in isolation.

A possible contributory role of *PHF10* and *DLL1* in causing the complex brain phenotype associated with the 6q terminal deletion may also be assumed. Indeed, *in utero* silencing of Phf10 and Dll1 did not cause PNH in our *in utero* electroporation experiments, but did produce slightly delayed neuronal migration. Though the function of these genes in brain development has not been fully elucidated, there is clear evidence that they play major roles on the proliferation of neuronal precursors. *Dll1* is involved in the switching from precursors to differentiated neurons (Kawaguchi *et al*., 2008). Neuronal differentiation is mediated mostly by the Notch signalling pathway (Louvi and Artavanis-Tsakona, 2006). Notch is a transmembrane receptor that is activated by the binding of ligands (including DLL1 in mammals) presented by neighbouring cells (Kawaguchi *et al*., 2008). In mice, different levels of *Dll1* expression determine the fate of neural precursor cells through cell–cell interactions, most likely through the Notch–Delta lateral inhibitory signalling pathway (Heitzler and Simpson, 1991; Heitzler *et al*., 1996). *In vivo* conditional deletion of *Dll1* in a small proportion of neuronal precursor cells reduced neurogenesis, whereas deletion in a large proportion of neuronal precursors promoted premature neurogenesis, suggesting that the regulation of *Dll1* expression should be critical in determining the place, timing and rate of neurogenesis (Kawaguchi *et al*., 2008). *Phf10* belongs to the neural progenitors-specific chromatin remodelling complex (npBAF complex) that is required for embryonic stem cell self-renewal and pluripotency (Ho *et al*., 2009; Yoo *et al*., 2009) and would eventually participate in the transition from proliferating neural stem/progenitor cells to post-mitotic neurons (Lessard *et al*., 2007). Therefore, *DLL1* and *PHF10* haploinsufficiency (or mutations) might affect cortical development and thus participate in the phenotype observed in patients with 6q terminal deletion. Overall, these data, in combination with our findings, led us to conclude that *C6orf70* plays a major role in causing PNH and that haploinsufficiency of contiguous genes *DLL1* and *PHF10* likely contributes to additional brain alterations observed in patients with 6q terminal deletion syndrome.

Acknowledgements

We gratefully acknowledge the patients and their families for participating in the research, Lucie Castelein and Dr. Christophe Pellegrino for their help and the High-Throughput Genomics Group at the Wellcome Trust Centre for Human Genetics for the generation of the sequencing data.

Funding

This work was supported by funding from the Sixth Framework Programme of the EU, project grant LSH-CT-2006-037315 (EPICURE) (to R.G., A.R. and C.C.), the European Research Projects on Rare Diseases (E-Rare-2, TUB-GENCODEV, 11-027) (to R.G.), the Oxford NIHR Biomedical Research Centre

Oxford and FWF grants P24367-B24 and I914-B13 (to D.A.K), INSERM (to A.R. and C.C.), the Health Research Council of New Zealand (to S.*P*.R.) and the Cure Kids New Zealand (to S.P.R.). A.C. is supported by a fellowship from FRM (Fondation pour la Recherche Medicale) and E.P.P. is a postdoctoral researcher supported by Else Kröner-Fresenius-Stiftung foundation (2010_A145). RJL and GM are supported by the Murdoch Children's Research Institute and the Victorian State Government Operational Infrastructure Support Program.

Supplementary material

Supplementary material is available at *Brain* on line

References

Backx L, Fryns JP, Marcelis C, Devriendt K, Vermeesch J, van Esch H. Haploinsufficiency of the gene Quaking (QKI) is associated with the 6q terminal deletion syndrome. Am J Med Genet A 2010; 152: 319–26.

Bai J, Ramos RL, Ackman JB, Thomas AM, Lee RV, LoTurco JJ. RNAi reveals doublecortin is required for radial migration in rat neocortex. Nat Neurosci 2003; 6: 1277–83.

Barkovich AJ, Guerrini R, Kuzniecky RI, Jackson GD, Dobyns WB. A developmental and genetic classification for malformations of cortical development: update 2012. Brain 2012; 135: 1348–69.

Bertini V, De Vito G, Costa R, Simi P, Valetto A. Isolated 6q terminal deletions: an emerging new syndrome. Am J Med Genet A 2006; 140: 74–81.

Carabalona A, Beguin S, Pallesi-Pocachard E, Buhler E, Pellegrino C, Arnaud K, et al. A glial origin for periventricular nodular heterotopia caused by impaired expression of Filamin-A. Hum Mol Genet 2012; 21: 1004–17.

Cardoso C, Boys A, Parrini E, Mignon-Ravix C, McMahon JM, Khantane S, et al. Periventricular heterotopia, mental retardation, and epilepsy associated with 5q14.3-q15 deletion. Neurology 2009; 72: 784–92.

Cellini E, Disciglio V, Novara F, Barkovich JA, Mencarelli MA, Hayek J, et al. Periventricular heterotopia with white matter abnormalities associated with 6p25 deletion. Am J Med Genet A 2012; 158A: 1793–7.

Dobyns WB, Mirzaa G, Christian SL, Petras K, Roseberry J, Clark GD, et al. Consistent chromosome abnormalities identify novel polymicrogyria loci in 1p36. 3, 2p16. 1–p23. 1, 4q21. 21–q22. 1, 6q26–q27, and 21q2. Am J Med Genet A 2008; 146: 1637–54.

Eash D, Waggoner D, Chung J, Stevenson D, Martin C. Calibration of 6q subtelomere deletions to define genotype/phenotype correlations. Clin Genet 2005; 67: 396–403.

Elia M, Striano P, Fichera M, Gaggero R, Castiglia L, Galesi O, et al. 6q terminal deletion syndrome associated with a distinctive EEG and clinical pattern: a report of five cases. Epilepsia 2006; 47: 830–8.

Ferland RJ, Gaitanis JN, Apse K, Tantravahi U, Walsh CA, Sheen VL. Periventricular nodular heterotopia and Williams syndrome. Am J Med Genet A 2006; 140: 1305–11.

Fox JW, Lamperti ED, Ekşioğlu YZ, Hong SE, Feng Y, Graham DA, et al. Mutations in filamin 1 prevent migration of cerebral cortical neurons in human periventricular heterotopia. Neuron 1998; 21: 1315–25.

Gerber JC, Neuhann TM, Tyshchenko N, Smitka M, Hackmann K. Expanding the clinical and neuroradiological phenotype of 6q27 microdeletion: olfactory bulb aplasia and anosmia. Am J Med Genet A 2011; 155: 1981–6.

Guerrini R, Dobyns WB, Barkovich AJ. Abnormal development of the human cerebral cortex: genetics, functional consequences and treatment options. Trends Neurosci 2008; 31: 154–62.

Guerrini R, Parrini E. Neuronal migration disorders. Neurobiol Dis 2010; 38: 154–66.

Heitzler P, Simpson P. The choice of cell fate in the epidermis of Drosophila. Cell 1991; 64: 1083–92.

Heitzler P, Bourouis M, Ruel L, Carteret C, Simpson P. Genes of the Enhancer of split and achaete-scute complexes are required for a regulatory loop between Notch and Delta during lateral signalling in Drosophila. Development 1996; 122: 161–71.

Hirose Y, Chiba K, Karasugi T, Nakajima M, Kawaguchi Y, Mikami Y, et al. A functional polymorphism in *THBS2* that affects alternative splicing and MMP binding is associated with lumbar-disc herniation. Am J Hum Genet 2008; 82: 1122–9.

Ho L, Ronan JL, Wu J, Staahl BT, Chen L, Kuo A, et al. An embryonic stem cell chromatin remodeling complex, esBAF, is essential for embryonic stem cell self-renewal and pluripotency. Proc Natl Acad Sci USA 2009; 106: 5181–6.

Jaleco AC, Neves H, Hooijberg E, Gameiro P, Clode N, Haury M, et al. Differential effects of Notch ligands Delta-1 and Jagged-1 in human lymphoid differentiation. J Exp Med 2001; 194: 991–1002.

Kawaguchi D, Yoshimatsu T, Hozumi K, Gotoh Y. Selection of differentiating cells by different levels of delta-like 1 among neural precursor cells in the developing mouse telencephalon. Development 2008; 135: 3849–58.

Lessard J, Wu JI, Ranish JA, Wan M, Winslow MM, Staahl BT, et al. An essential switch in subunit composition of a chromatin remodeling complex during neural development. Neuron 2007; 55: 201–15.

Liu G, Thomas L, Warren RA, Enns CA, Cunningham CC, Hartwig JH, et al. Cytoskeletal protein ABP-280 directs the intracellular trafficking of furin and modulates proprotein processing in the endocytic pathway. J Cell Biol 1997; 139: 1719–33.

Louvi A, Artavanis-Tsakonas S. Notch signalling in vertebrate neural development. Nat Rev Neurosci 2006; 7: 93–102.

Lunter G, Goodson M. Stampy: a statistical algorithm for sensitive and fast mapping of Illumina sequence reads. Genome Res 2011; 21: 936–9.

Moro F, Pisano T, Dalla Bernardina B, Polli R, Murgia A, Zoccante L, et al. Periventricular heterotopia in fragile X syndrome. Neurology 2006; 67: 713–5.

Neal J, Apse K, Sahin M, Walsh CA, Sheen VL. Deletion of chromosome 1p36 is associated with periventricular nodular heterotopia. Am J Med Genet A 2006; 140: 1692–5.

Neesen J, Drenckhahn JD, Tiede S, Burfeind P, Grzmil M, Konietzko J, et al. Identification of the human ortholog of the t-complex-encoded protein TCTE3 and evaluation as a candidate gene for primary ciliary dyskinesia. Cytogenet Genome Res 2002; 98: 38–44.

Pagnamenta AT, Lise S, Harrison V, Stewart H, Jayawant S, Quaghebeur G, et al. Exome sequencing can detect pathogenic mosaic mutations present at low allele frequencies. J Hum Genet 2012; 57: 70–2.

Parrini E, Ramazzotti A, Dobyns W, Mei D, Moro F, Veggiotti P, et al. Periventricular heterotopia: phenotypic heterogeneity and correlation with Filamin A mutations. Brain 2006; 129: 1892–1906.

Pisano T, Barkovich AJ, Leventer RJ, Squier W, Scheffer IE, Parrini E, et al. Peritrigonal and temporo-occipital heterotopia with corpus callosum and cerebellar dysgenesis. Neurology 2012; 79: 1244–51.

Schwarz-Romond T, Merrifield C, Nichols BJ, Bienz M. The Wnt signalling effector dishevelled forms dynamic protein assemblies rather than stable associations with cytoplasmic vesicles. J Cell Sci 2005; 118: 5269–77.

Sheen V, Wheless J, Bodell A, Braverman E, Cotter P, Rauen K, et al. Periventricular heterotopia associated with chromosome 5p anomalies. Neurology 2003; 60: 1033–6.

Sheen VL, Basel-Vanagaite L, Goodman JR, Scheffer IE, Bodell A, Ganesh VS, et al. Etiological heterogeneity of familial periventricular heterotopia and hydrocephalus. Brain Dev 2004; 26: 326–34.

Sheen VL. Periventricular heterotopia: shuttling of proteins through vesicles and actin in cortical development and disease. Scientifica 2012; 2012: Article ID 480129, doi:10.6064/2012/480129.

Shin HW, Shinotsuka C, Nakayama K. Expression of BIG2 and analysis of its function in mammalian cells. Methods Enzymol 2005; 404: 206–15.

Stevenson DA, Brothman AR, Carey JC, Chen Z, Dent KM, Bale JF Jr, et al. 6q subtelomeric deletion: is there a recognizable syndrome? Clin Dysmorphol 2004; 13: 103.

Stossel TP, Condeelis J, Cooley L, Hartwig JH, Noegel A, Schleicher M, et al. Filamins as integrators of cell mechanics and signalling. Nat Rev Mol Cell Biol 2001; 2: 138–45.

Striano P, Malacarne M, Cavani S, Pierluigi M, Rinaldi R, Cavaliere ML, et al. Clinical phenotype and molecular characterization of 6q terminal deletion syndrome: five new cases. Am J Med Genet A 2006; 140: 1944–9.

Sverdlov M, Shinin V, Place AT, Castellon M, Minshall RD. Filamin A regulates caveolae internalization and trafficking in endothelial cells. Mol Biol Cell 2009; 20: 4531–40.

van der Flier A, Sonnenberg A. Structural and functional aspects of filamins. Biochim Biophys Acta 2001; 1538: 99–117.

van Kogelenberg M, Ghedia S, McGillivray G, Bruno D, Leventer R, MacDermot K, et al. Periventricular heterotopia in common microdeletion syndromes. Mol Syndromol 2010; 1: 35–41.

Xu B, Roos JL, Dexheimer P, Boone B, Plummer B, Levy S, et al. Exome sequencing supports a de novo mutational paradigm for schizophrenia. Nat Genet 2011; 43: 864–8.

Yoo AS, Staahl BT, Chen L, Crabtree GR. MicroRNA-mediated switching of chromatin-remodelling complexes in neural development. Nature 2009; 460: 642–6.

Yu JY, DeRuiter SL, Turner DL. RNA interference by expression of short-interfering RNAs and hairpin RNAs in mammalian cells. Proc Natl Acad Sci USA 2002; 99: 6047.